Grain segregation mechanism in aeolian sand ripples

H.A. Makse[a]

Schlumberger-Doll Research, Old Quarry Road, Ridgefield, CT 06877, USA

Abstract. Many sedimentary rocks are formed by migration of sand ripples. Thin layers of coarse and fine sand are present in these rocks, and understanding how layers in sandstone are created has been a longstanding question. Here, we propose a mechanism for the origin of the most common layered sedimentary structures such as inverse graded climbing ripple lamination and cross-stratification patterns. The mechanism involves a competition between three segregation processes: (i) size-segregation and (ii) shape-segregation during transport and rolling, and (iii) size segregation due to different hopping lengths of the small and large grains. We develop a discrete model of grain dynamics which incorporates the coupling between moving grains and the static sand surface, as well as the different properties of grains, such as size and roughness, in order to test the plausibility of this physical mechanism.

PACS. 81.05.Rm Porous materials; granular materials – 91.65.Ti Sedimentary petrology

1 Introduction

Subject to the effects of wind, a flat sandy surface is unstable and evolves into a regular periodic pattern of wavelength of the order of 10 cm and height of a few centimeters (see Fig. 1) [1–9]. A slight sand accumulation on the surface tends to expose grains on the upwind stoss-side to the action of the wind, and shelter the grains on the downwind lee-side. Dislodged grains at the stoss tend to move toward the lee of the sand accumulation, the initial perturbation is amplified, and small ripples develop, which migrate in the direction of the wind. Smaller ripples travel faster than larger ripples – since the migration velocity of ripples depends on the amount of grains being transported during migration – so that small ripples merge with the larger ones. Due to ripple merging, the wavelength of the ripples grows in time as observed in the field [2,10] and in wind tunnel experiments [11,12].

Due to the action of the wind, grains fly above the bed and strike the ground at small angles and with velocities given by the wind velocity. Successive impacts of grains are called *saltation*. As a result of bombardment of saltating grains, a number of ejected grains are generated from the static bed which subsequently move by surface creep. These grains (called *reptating* grains) move distances smaller than the typical saltating jump (which is controlled by the wind velocity) until they are captured and become part of the bed.

Climbing of ripples as seen in Figure 2 is described by a vector of translation which has two components [6]: the component in the horizontal direction is the rate of ripple migration across the sediment surface, and the component

Fig. 1. Wind sand ripples on a sandy surface in Death Valley National Park, California.

in the vertical direction is the net rate of deposition, defined as the rate of displacement of the sand surface in the vertical direction (see Fig. 3a). The angle of climbing (ξ in Fig. 3a) defines different types of lamination structures (see Chap. 9 in [7]). If the angle of climb is smaller than the slope of the stoss, then the structures are called "subcritically" climbing ripples, and these are the sedimentary structures which are the focus of this study.

Due to the climbing of ripples and segregation of grains during deposition and transport, ripple deposits develop lamination structures which are later preserved during solidification of the rock [3,6,7]. The basic types of the smallest stratification structures in climbing ripples and small aeolian dunes relevant to this study are summarized by
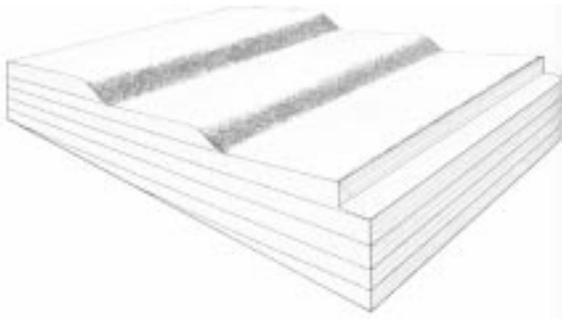
[a] e-mail: `makse@ridgefield.sdr.slb.com`

Fig. 2. Diagram showing the climbing of the ripples and the formation of cross-stratification patterns (from [5]).

Hunter [3] (see also [7]). In this paper we will focus on two lamination structures which are commonly found in sedimentary rocks.

– Inverse-graded climbing ripple lamination: one of the most common lamination structures which are formed because grains composing the ripples differ in size [1,3,7,13]. Large ejected grains travel in shorter trajectories than small grains, so that small grains are preferentially deposited in the trough of the ripples while large grains are deposited preferentially near the crest. Due to this segregation effect, the migration of a single ripple produces two layers of different grain size parallel to the climbing direction of the ripple as shown in Figure 3a. This lamination structure is called inverse-graded – according to the nomenclature of Hunter [3] – since in a pocket of two consecutive layers formed by the climbing of a single ripple, the layer of large grains is above the layer of small grains (Fig. 3a).
– Cross-stratification: migration of ripples also produces successive layers of fine and coarse grains not in the direction of climbing but parallel to the downwind face of the ripples (see Figs. 2 and 3b) [1,3,5–8]. These structures – called cross-stratification or foresets – are also coarser toward the troughs [1,14–16] as opposed to the segregation in inverse-graded climbing ripples.

The instability giving rise to aeolian ripple morphologies has been the subject of much study. The classic work of Bagnold [1] has been followed up by a number of studies. Modern models of wind ripple deposits are usually defined in terms of the splash functions introduced by Haff and coworkers [17,18] (see also [12] for a review) in order to model impact processes. These models have successfully reproduced the instability leading to ripple deposits when the sand grains are of only one size [12,19,20]. When such models are defined for two species of grains differing in size [13], they result in patterns which resemble very closely the stratigraphic patterns found in inverse grading climbing ripple structures. It was in this context that Forrest and Haff proposed [19] that grading changes in ripple lamination are related to fluctuations in wind or transport. However, Anderson and Bunas [13] found using a cellular automaton model that inverse-graded ripple lamination is due to different hopping lengths of small and large grains. These models do not include the interactions

(a) Inverse grading climbing ripples
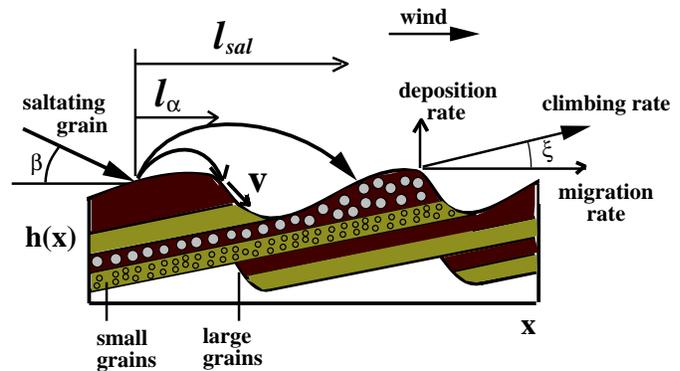
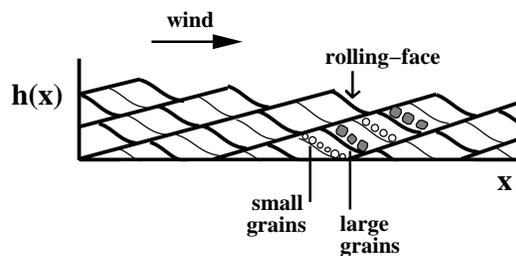**(b) Cross–stratification**

Fig. 3. (a) Cross-section of a sandstone showing small-scale lamination in "subcritically" (as defined in [3,7]) inverse-graded ripples (along with the quantities defined in the model). Each pair of layers of small and large grains is produced by the climbing of a single ripple. (b) Example of cross-stratification. Each climbing ripple produces a series of layers of small and large grains oriented across the direction of climbing, parallel to the downwind face. The basic types of the smallest stratification structures in ripples and small aeolian dunes relevant to this study are summarized in [3].

between the moving grains and the static surface [20] – *i.e.*, grains are assumed to stop as soon as they reach the sand surface – which are expected to be relevant for the dynamics in the rolling face of the ripples [21,22]. Recent studies by Terzidis *et al.* [22] have reproduced the ripple instability using the theory of surface flows of grains proposed by Bouchaud and collaborators [23]. This theory takes into account the interaction between rolling and static grains. Moreover, recent studies of avalanche segregation of granular mixtures show dramatic effects when such interactions are taken into account [24,25].

In this article, we use this formalism to include also the segregation effects arising when considering two types of species of different size and shape. We first formulate a discrete model for two-dimensional transverse aeolian climbing ripples which incorporates simple rules for hopping and transport. Then, we incorporate the different properties of the grains, such as size and roughness, and we show that pattern formation in ripple deposits arises as a consequence of grain segregation during the flow

Segregation due to different hopping lengths
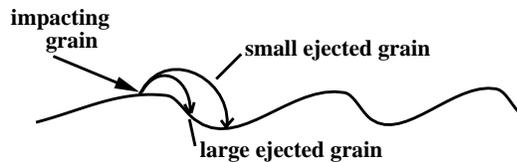
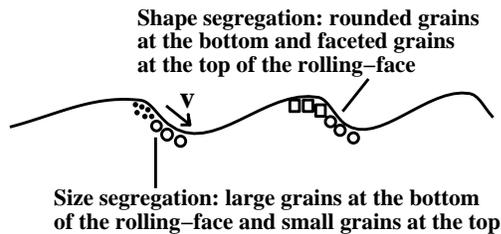
Segregation in the rolling face

Fig. 4. Three segregation mechanisms acting when the grains differ in size and shape.

and collisions. Specifically we show that three segregation mechanisms contribute to layer formation during ripple migration (Fig. 4):

– size segregation due to different hopping lengths of small and large grains: the hopping length of the large reptating grains is smaller than the hopping length of small grains;

– size segregation during transport and rolling: larger grains tend to roll down to the bottom of troughs while small grains tend to be stopped preferentially near the crest of ripples;

– shape segregation during transport and rolling: rounded grains tend to roll down easier than more faceted or cubic grains, so that the more faceted grains tend to be at the crest of the ripples, and more spherical grains tend to be near the bottom.

As a result of a competition between these segregation mechanisms a richer variety of stratigraphic patterns emerges: inverse-graded ripple lamination occurs when segregation due to different jump lengths dominate, and cross-stratification (and normal-graded ripple lamination as well) occurs when size and shape segregation during rolling dominates. Thus, a general framework is proposed to unify the mechanisms underlying the origin of the most common wind ripple deposits. In the case of inverse-graded climbing ripple lamination we confirm a previously formulated hypothesis by Bagnold [1] and Anderson and Bunas [13] that the lamination is due to hopping induced segregation due to collisions. Regarding the origin of cross-stratification structures, we show that they arise under similar conditions as in recent table-top experiments of avalanche segregation of mixtures of large faceted grains and small rounded grains poured in a vertical Hele-Shaw cell [16, 24].

In what follows we first define the model for the case of single species of grains. We show that the model predicts the formation of a ripple structure, and propose a simplified continuum theory to understand the onset of the stability leading to ripple structure. Then, we generalize the model to the case of two type of species of grains differing in size and shape which give rise to the segregation mechanisms and the lamination structures seen in aeolian climbing ripples.

2 One species model

We start by defining the model for the case of one type of grain in a two-dimensional lattice of lateral size L with periodic boundary conditions in the horizontal x-direction. Our main assumption is to consider two different phases [22–26]: a reptating or rolling phase composed by grains moving with velocity v by rolling, and a static phase composed by grains in the bulk. We also consider a curtain of external saltating grains which impact – at randomly chosen positions on the static surface – from the left to the right at a small angle β to the horizontal (Fig. 3a). Shadow effects are considered by allowing only impacts with ballistic trajectories which do not intersect any prior portion of the surface. Upon impacting on the sand surface, a saltating grain dislodges n_{rep} grains from the static surface, and jumps a distance l_{sal} after which the saltating grain is incorporated to the reptating phase. The n_{rep} grains dislodged by the saltating grain jump a distance $l_{\mathrm{rep}} \ll l_{\mathrm{sal}}$. Upon reaching the surface, the dislodged grains form part of the reptating phase and move with velocity v.

At every time step (Δt) only one reptating grain (in contact with the surface) interacts with the static grains of the bulk according to the angle of repose θ_{r} [27]; the remaining reptating grains move a distance $v\Delta t$ to the right. The angle of repose is the maximum angle at which a reptating grain is captured on the sand bed. If the local coarse-grained angle of the surface is smaller than the angle of repose, $\theta < \theta_{\mathrm{r}}$, the interacting reptating grain will stop and will be converted into a static grains. If the angle of the surface is larger than the angle of repose, $\theta > \theta_{\mathrm{r}}$, the reptating grain is not captured – and moves to the right a distance $v\Delta t$ with the remaining reptating grains – but ejects a static grain from the bulk into the reptating phase.

The model predicts the formation of a ripple structure as seen in aeolian sand formations. The onset of the instability leading to ripples occurs with ripples of small wavelength. However, due to the fact that smaller ripples travel faster than larger ripples – since smaller ripples have less amount of material to transport – merging of small ripples on top of large ripples is observed. This gives rise to the change of the characteristic wavelength as a function of time, as is observed in wind tunnel experiments [11, 12], as well as in field observations [2, 10]. We find that our model predicts an initial power law growth of the wavelength of the ripples $\lambda(t) \sim t^{0.4}$ (see Fig. 5). The wavelength of the ripples seems to saturate after this power law growth to a value determined by the saltating length. Moreover,
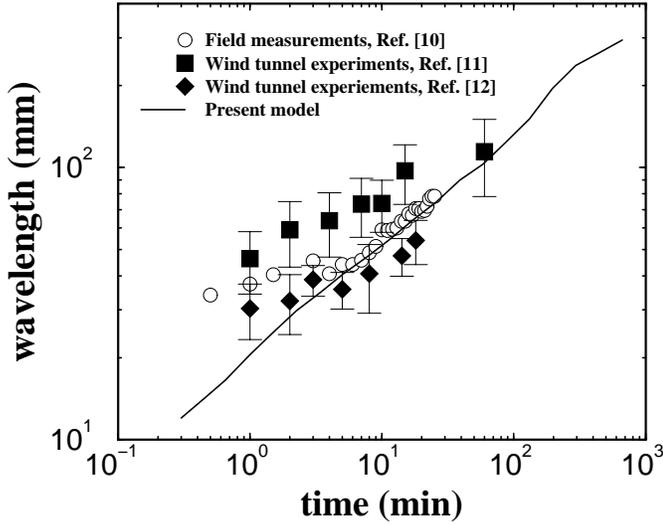
Fig. 5. Growth of the wavelength of the ripples according to our model and comparison with field and experimental observations. The number of impacts in the model is translated to time using a typical impact rate of 10^7 impacts $\mathrm{m}^{-2}\,\mathrm{s}^{-1}$ [12]. The simulation data have been shifted vertically by a multiplicative factor, so that only the general trend (the slope) of the curve should be compared with the experimental data.

we also observe a subsequent growth of the wavelength (not shown in the figure) up to a new saturation value close to a multiple of the saltation length. This process continues and a series of plateaus are observed until one large ripple (or dunes) of the size of the system is formed. The series of plateaus was also observed in a recent lattice model of ripple merging [28]. However, we believe that the existence of plateaus might be due to an artifact of the discreteness of the lattice, and may have no physical meaning: the rules associated with the derivatives of the sand surface break down when the local slope is bigger than a given value determined by the discretization used to define the slope of the surface. A similar artifact was observed in a discrete model of ripple morphologies formed during surface erosion *via* ion-sputtering in amorphous materials [29]. Moreover, we will see that when we introduce two species of grains, the wavelength saturates at a constant value and the plateaus disappear.

In Figure 5 we compare the prediction of our model with the available experimental data from field and wind tunnel experiments. We observe a fair agreement between our model and the experiments. However, we believe that this agreement is not conclusive. In fact, the same experimental data can be also fitted with the same accuracy by a logarithmic growth of the wavelength of the ripples as shown recently by Werner and Gillespie [10], who proposed a discrete stochastic model of ripple merging and found a logarithmic growth of the wavelength (see also [28]).

Continuum formulation of the model

The onset of the instability leading to the initial ripple structure can be studied using the continuum theory proposed by Bouchaud *et al.* [23] to study avalanche in sandpiles. Recently, the set of coupled equations for surface flow of grains of [23] has been adapted to the problem of the ripple instability [22]. Here, we propose a version of this theoretical formalism suitable to the physics of our model to study the initial ripple formation. Let $R(x,t)$ describe the amount of reptating grains in the rolling phase and $h(x,t)$ the height of the static bed at position x and time t, which is related to the angle of the sand surface by $\theta(x,t) \equiv -\partial h/\partial x$ for small angles. Our set of convective-diffusion equations for the rolling and static phases are the following [23]:

$$\frac{\partial R(x,t)}{\partial t} = -v\frac{\partial R}{\partial x} + D\frac{\partial^2 R}{\partial x^2} + \Gamma(R,\theta), \qquad (1a)$$

$$\frac{\partial h(x,t)}{\partial t} = -\Gamma(R,\theta), \qquad (1b)$$

where v is the drift velocity of the reptating grains along the positive x axis taken to be constant in space and time, and D a diffusion constant. The interaction term Γ takes into account the conversion of static grains into rolling grains, and *vice versa*. We propose the following form of Γ consistent with our model:

$$\Gamma(R,\theta) \equiv \alpha[\beta - \theta(x,t)] + \gamma[\theta(x,t) - \theta_{\mathrm{r}}]R(x,t), \qquad (2)$$

where α and γ are two constants with dimension of velocity and frequency respectively. α is proportional to the number of collisions per unit time of the saltating grains with the sand bed, and also to the number of ejected grains per unit time, while γ is the number of collisions per unit time between the reptating grains and the sand bed when they creep on the downwind side of the ripple. The first term in (2) takes into account the spontaneous (independent of $R(x,t)$) creation of reptating grains due to collisions of the saltating grains – a process which is most favorable at angles of the bed smaller than β. The second term takes into account the interaction of the reptating grains with the bed of static grains: the rate of the interaction is proportional to the number of grains $R(x,t)$ interacting with the sand surface. Rolling grains become part of the sand surface if the angle of the surface $\theta(x,t)$ is smaller than the repose angle θ_{r} ("capture"), while static grains become rolling grains if $\theta(x,t)$ is larger than θ_{r} ("amplification"). Higher order terms are neglected since we are interested in the linear stability analysis determining the origin of the ripple instability.

Insight into the mechanism for ripple formation is obtained by studying the stability of the uniform solution of equations (1a, 1b):

$$R_0 = \alpha\beta/(\gamma\theta_{\mathrm{r}}) \quad h_0 = 0. \qquad (3)$$

We perform a stability analysis by looking for solutions of the type: $R(x,t) = R_0 + \bar{R}(x,t)$ and $\theta(x,t) = \theta_0 + \bar{\theta}(x,t)$.

The linearized equations for $\bar{R}$ and $\bar{\theta}$ are

$$\frac{\partial \bar{R}(x,t)}{\partial t} = -v\frac{\partial \bar{R}}{\partial x} - v_{\mathrm{m}}\bar{\theta} - \gamma\theta_{\mathrm{r}}\bar{R} + D\frac{\partial^2 \bar{R}}{\partial x^2}, \qquad (4a)$$

$$\frac{\partial \bar{\theta}(x,t)}{\partial t} = -v_{\mathrm{m}}\frac{\partial \bar{\theta}}{\partial x} - \gamma\theta_{\mathrm{r}}\frac{\partial \bar{R}}{\partial x}, \qquad (4b)$$

where the migration velocity of the traveling wave solution is

$$v_{\mathrm{m}} = \alpha(1 - \beta/\theta_{\mathrm{r}}), \qquad (5)$$

which indicates that the ripple velocity is proportional to the number of collisions per unit unit of saltating grains with the sand bed, and to the number of ejected grains per collision.

By Fourier analyzing equations (4a, 4b) we find a set of two homogeneous algebraic equations for $\bar{R}$ and $\bar{\theta}$ with non-trivial solutions only when the determinant of the resulting 2×2 matrix is zero. We obtain a dispersion relation $w_{\pm}(k)$ where the two branches $\pm$ correspond to the solutions of the resulting quadratic equation for $w(k)$. Then we take the limit $v_{\mathrm{m}}/v \ll 1$, which corresponds to the physical fact that the translation velocity (5) is much smaller than the rolling velocity of the individual grains (see [22]), and we arrive to the following dispersion relation for $w_{-}(k)$ ($w_{+}(k)$ gives rise only to stable modes):

$$\mathrm{Im}[w_{-}(k)] = \frac{-(v_{\mathrm{m}}/v)(\gamma\theta_{\mathrm{r}}v^2)k^2}{(\gamma\theta_{\mathrm{r}})^2 + k^2(2\gamma\theta_{\mathrm{r}}D + v^2) + D^2k^4} + O(\frac{v_{\mathrm{m}}}{v})^2. \qquad (6)$$

The asymptotic forms for small and large k are

$$\mathrm{Im}[w_{-}(k)] \to -\frac{v_{\mathrm{m}}v}{\gamma\theta_{\mathrm{r}}}k^2, \quad k \to 0$$

$$\mathrm{Im}[w_{-}(k)] \to -\frac{v_{\mathrm{m}}v\gamma\theta_{\mathrm{r}}}{D^2}\frac{1}{k^2}, \quad k \to \infty \qquad (7)$$

which indicates that the branch $w_{-}(k)$ corresponds to only unstable modes $w_{-}(k) < 0$. Similar stability analysis was performed by Anderson [20] using a continuity model neglecting the interaction between rolling and static grains and by Terzidis *et al.* [22] with the continuum model equations (1a, 1b) but with a different interaction term than equation (2). Terzidis *et al.* find a band of unstable modes until a given cut off wave vector at large k. This behaviour is due to higher order derivatives of θ appearing in the interaction term used in [22]. The most unstable mode k^* in our model is given by $\partial w_{-}(k^*)/\partial k = 0$, with $k^* = \sqrt{\gamma\theta_{\mathrm{r}}/D}$ which gives an estimate of the initial wavelength of the ripples:

$$\lambda = 2\pi\sqrt{D/(\gamma\theta_{\mathrm{r}})}. \qquad (8)$$

The final wavelength will be determined by higher order nonlinear terms arising from a more complicated interaction term than the one used in equation (2). As mentioned above, using the full discrete model we find that after the appearance of initial small undulations, the wavelength of the ripples grows due to ripple merging. In the discrete model, the wavelength seems to saturate to a finite value, although this value seems to be determined by the finite size of the simulation system (we use periodic boundary conditions in the horizontal direction).

3 A model for two species differing in size and shape

Next we generalize the model to the case of two type of species differing in size and shape. The segregation mechanisms discussed in the introduction are incorporated in the model as follows:

– size segregation due to different hopping lengths: we define l_{α} (to replace l_{rep} of the mono disperse case) as the distance a reptating grain of type α travels after being collided by a saltating grain. If we call the small grains type s and the large grains type l, then $l_l < l_s$. This effect was incorporated in the discrete stochastic model of Anderson and Bunas [13] using a generalization of the splash functions proposed by Haff [18].

The interaction between the rolling grains and the surface is characterized by four different angles of repose; $\theta_{\alpha\beta}$ for the interaction of an α reptating grain and a β static grain (replacing θ_{r} of the mono disperse case). The dynamics introduced by the angle of repose are relevant at the downwind face where two extra mechanisms for segregation of grains act in the system:

– size segregation during transport and rolling: large rolling grains are found to rise to the top of the reptating phase while the small grains sink downward through the gaps left by the motion of larger grains; an effect known as percolation or kinematic sieving [1,30]. Due to this effect only the small grains interact with the surface when large grains are also present in the rolling phase. Small grains are captured first near the crest of the ripples causing the larger grains to be convected further to the bottom of the ripples. We incorporate this dynamical segregation effect by considering that, when large and small grains are present in the reptating phase, only the small ones interact with the surface according to the angle of repose, while the large grains, being at the top of the reptating phase do not interact with the static grains and they are convected downward. Thus, the large grains interact with the surface only when there are no small grains present in the reptating phase. A similar percolation mechanism was introduced in the discrete and continuum models of [24] to understand the origin of stratification patterns in two-dimensional sandpiles of granular mixtures;
– shape segregation during transport and rolling: rounded grains tend to roll down easier than more faceted or cubic grains, so that the more faceted grains tend to be at the crest of the ripples. This segregation effect is quantified by the angles of repose of the pure

species, since the repose angle is determined by the shape and surface properties of the grains and not by their size: the rougher or the more faceted the surface of the grains the larger the angle of repose. If the large grains are more faceted than the small grains we have $\theta_{ss} < \theta_{ll}$, while when the small grains are more faceted $\theta_{ll} < \theta_{ss}$ [24]. The species with the larger angle of repose have a larger probability to be captured at the sand bed than the species with smaller angle of repose.

We notice that the fact that the grains have different size leads to different cross-angles of repose $\theta_{\alpha\beta}$ [24,31]. If the large grain are type l and the small are type s then $\theta_{ls} < \theta_{sl}$, which in turn leads to another size segregation effect. However, by incorporating the size segregation due to the different cross-angle of repose we would get the same effect as the one incorporated in the model by the percolation effect (the small grains are preferentially trapped at the top of the slip-face), so that, in what follows, we will consider only the percolation effect for simplicity – *i.e.*, large reptating grains are allowed to interact with the sand surface only when there are no small reptating grains below the large grains at a given position.

We also notice that, in general, the distance a grain travels after being kicked by a saltating grain depends on the type of colliding grain and the type of grain on the bed. Thus we define $l_{\alpha\beta}$ as the distance a reptating grain of type β travel after being collided by a saltating grain of type α. If we call the large grains type l and the small grains type s then we have: $l_{sl} < l_{ll} < l_{ss} < l_{ls}$. Hoverer, in practice we will make the following approximation $l_{sl} = l_{ll} \equiv l_l$, and $l_{ss} = l_{ls} \equiv l_s$, *i.e.*, we do not consider which type of grain is colliding.

Thus, three different mechanisms – size-segregation due to percolation in the reptating phase, shape-segregation in avalanches, and size segregation due to the different reptating jumps l_α – compete in the system giving rise to a rich variety of lamination patterns as we show below.

3.1 Size segregation due to different hopping lengths

We first investigate the morphologies predicted by the model in the case where the different reptating jumps l_α play the dominant role in the segregation process. This is the case $l_s - l_l > l_s$ and when the grains have approximately the same shape $\theta_{ss} \approx \theta_{ll}$. We start our simulations from a flat sand surface composed by a 50/50 by volume mixture of small and large grains and we observe the system to evolve into ripples traveling in the direction of the wind (Fig. 6). The resulting morphology seen in Figure 6 resembles the most common climbing ripple structures such as those documented in field observations [3,6–8] (Fig. 3a). This result confirms the hypothesis of Anderson and Bunas [13] that the origin of inverse-graded lamination in climbing ripples is due to the size segregation effect produced by the different hopping lengths of small and large grains. In our simulations we observe that

Inverse graded lamination

Fig. 6. Morphology predicted by the model when segregation due to different jump lengths is dominant showing inverse grading climbing ripple lamination. From left to right, we show a sequence of three stages in the dynamics of the climbing ripples. Starting from a flat sand surface of small (light color) and large grains (dark color), the system evolves into ripples climbing in the direction of the wind.

large grains (dark color) are deposited at the top of the ripples while small grains (light color) are deposited preferentially at the bottom of the ripples since $l_l < l_s$, resulting in a lamination structure showing inverse grading (layer of large grains on top of the layer of small grains).

The system size used in our simulations corresponds to 256 bins, with $\Delta t = 1$ s, $n_{\rm rep} = 4$ grains per impact, $l_{\rm sal} = 90$ cm, $\beta = 10°$. For the case shown in Figure 6 we use $l_1 = 25$ cm and $l_2 = 5$ cm, and $\theta_{\alpha\beta} = 30°$.

The efficiency of the segregation mechanisms is sensitive to the relative value of the parameters of the model. For instance we find that by decreasing the value of $l_{\rm sal}$ relative to the reptating lengths, the efficiency of segregation is greatly reduced in the case of inverse-graded lamination. The structures shown here are all subcritically climbing from left to right (for a review of the terminology and definition of different climbing structures in ripples deposit see [3], and Chap. 9 in [7]). Supercritical climbing ripples are much less common and are produced in slowly translating ripples with small number of ejected grains per impact [19]. We also notice that the shape of ripples found in Nature are more asymmetric with the downwind side at a steeper angle than the upwind side, while our model predicts a more symmetric triangular shape of the ripples. More realistic asymmetric shape of the ripples can be obtained by considering the exact trajectories of the flying grains and the complex interaction of grains with the air flow as shown by previous models by Anderson [13].

3.2 Segregation due to rolling and transport

Next we consider the case where the difference between the reptating jumps is small, $|l_s - l_l|/l_s < 1$ (or when the downwind face is large compared to l_s or l_l) and the grains differ appreciable in shape ($\theta_{ss} \neq \theta_{ll}$) and also in size. Then segregation in the rolling face is the relevant mechanism for segregation and we do not take into account the segregation due to different hoping lengths.

We first consider the case where the small grains are the roughest and the large grains are the most rounded ($\theta_{ss} > \theta_{ll}$). In this case a segregation solution along the downwind face is possible since both, size segregation due to percolation and shape segregation act to segregate the

(a) Normal graded lamination
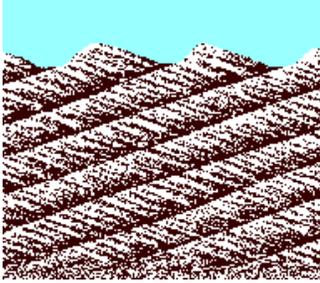

(b) Cross-stratification

Fig. 7. Resulting morphologies predicted by the model after 10^7 impacts, when segregation in the rolling face is dominant showing (a) normal grading lamination of large rounded grains (dark color, at the bottom of the downwind face) and small rough grains (light color, at the top); and (b) cross-stratification of large rough grains (dark color) and small rounded grains (light color).

small-faceted grains at the top of the crest and the large-rounded grains at the bottom of troughs. The result is a lamination structure (Fig. 7a) which resembles the structure of climbing ripples of Figure 6 but with the opposite grading: small grains at the top of each pair of layers (normal-grading climbing ripple lamination). This type of lamination is not very common in Nature.

On the other hand, when the large grains are rougher than the small grains ($\theta_{ll} > \theta_{ss}$), a competition between size and shape segregation occurs [32]. Size segregation due to percolation tends to segregate the large-cubic grains at the bottom of the downwind face, while the shape segregation effect tends to segregate the same grains at the crest of the ripples. Then a segregation solution along the downwind face as in Figure 7a is not possible, and the result of this instability is the appearance of layers of small and large grains parallel to the downwind face (Fig. 7b) and not perpendicular as in Figure 7a. These structures correspond to the more common cross-stratification patterns found in rocks [3,6–8]. In addition to the stratification parallel to the rolling face, the deposits are also coarser toward the bottom of the downwind face.

The mechanism for cross-stratification involves two phenomena superimposed.

(i) Segregation in the rolling face: a pair of layers is laid down in a single rolling event, with the small grains segregating themselves underneath the larger grains

through a "kink" mechanism as seen in [16,24]. This kink in the local profile of static grains provides local stability to the rolling grains trapping them. The kink moves uphill forming layers of small and large grains.

(ii) The climbing of ripples due to grain deposition and ripple migration.

The conditions for cross-stratification and the dynamical segregation process found with the present model are similar to the findings of the experiments of stratification of granular mixtures in two-dimensional vertical cells performed in [16] and also the models of [24]. We observe the formation on the slip face of the ripples of an upward traveling wave or "kink" at which grains are stopped during the avalanche as was observed in [16,24]. According to this, the wavelength of the layers is proportional to the flux of grains reaching the rolling face, then it is proportional to the number of saltating grains impacting the surface.

For the case shown in Figure 7a we use $l_s = l_l = 5$ cm, and $\theta_{sl} = \theta_{ss} = 30°$, and $\theta_{ls} = \theta_{ll} = 20°$, while for Figure 7b we use $l_s = l_l = 5$ cm, and $\theta_{sl} = \theta_{ss} = 20°$, and $\theta_{ls} = \theta_{ll} = 30°$.

3.3 Phase diagram: General case

We have also investigated the morphologies obtained when the three segregation effects (shape segregation, percolation effect, and hopping induced size segregation) act simultaneously. The resulting morphologies are shown in Figure 8 along with the phase diagram summarizing the results obtained with the model in Figures 6 and 7.

The case $|l_s - l_l| > l_s$ and $\theta_{ss} \approx \theta_{ll}$ corresponds to the inverse-graded lamination shown in Figure 6, as indicated in the phase diagram Figure 8. Moreover, when $l_s - l_l > l_s$ and for any other value of the angles θ_{ss} and θ_{ll}, we find that the hopping induced segregation seems to dominate over rolling induced segregation. As can be seen from the upper two panels in Figure 8, the morphologies obtained in these cases resemble the one of Figure 6 corresponding to inverse-graded climbing ripple lamination. The upper left panel shows the results when the smaller grains are the roughest $\theta_{ll} - \theta_{ss} < 0$ and shows clearly the same lamination as in Figure 6. In this case the hopping induced segregation dominates completely over the rolling segregation due to the angles of repose and percolation. In the upper right panel we show the case when the large grains are the roughest $\theta_{ll} - \theta_{ss} > 0$. In this case we also see the same lamination pattern as in Figure 6 but we see a tenuous trace of the cross-stratification seen in Figure 7b too; the rolling induced segregation seems to have a more important role in comparison with the hopping induced segregation than in the case shown in the upper left panel.

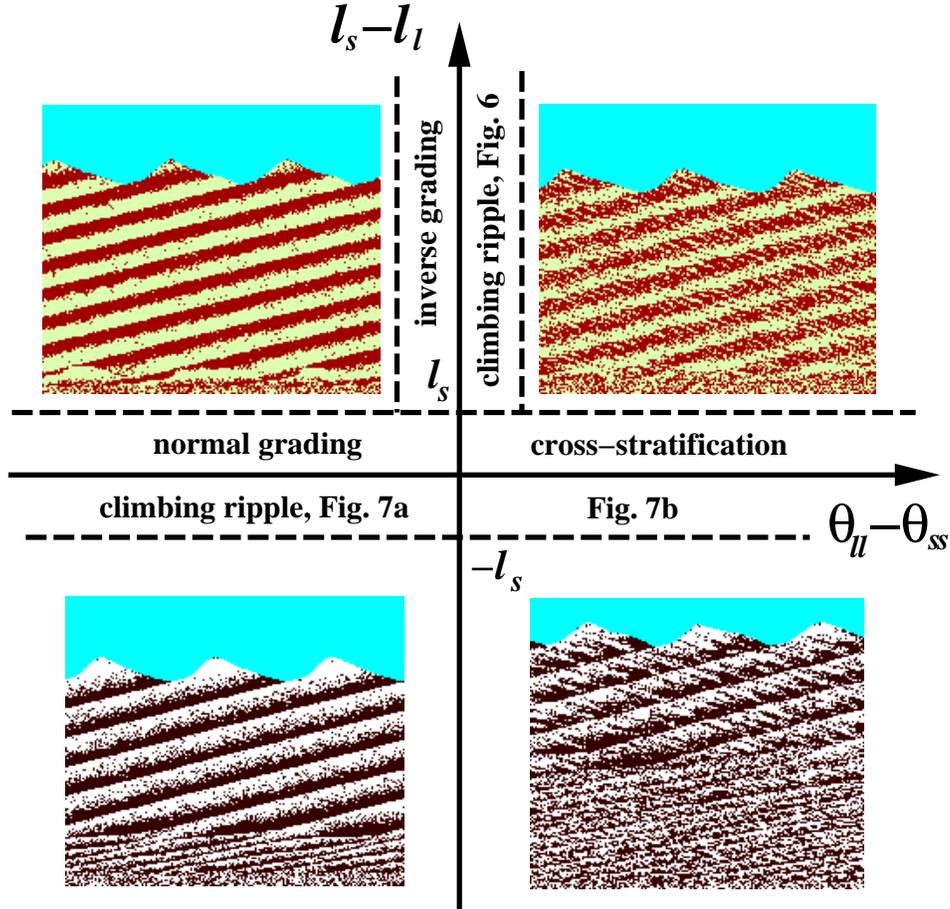The region $|l_s - l_l| < l_s$ is discussed in Figure 7, and our model shows normal grading lamination when $\theta_{ll} - \theta_{ss} < 0$ (Fig. 7a) and cross-stratification when $\theta_{ll} - \theta_{ss} > 0$ (Fig. 7b).

Fig. 8. Phase diagram predicted by the model. The "s" refers to the small grains (light colors), and the "l" refers to the large grains (dark colors). $\theta_{ss} > \theta_{ll}$ means that the smaller grains are the roughest, and $\theta_{ll} > \theta_{ss}$ means that the larger grains the roughest. The three areas in the phase space near the axis refer to the morphologies already studied in Figures 6, 7a and 7b.

Interesting morphologies are predicted when $l_s - l_l < -l_s$. This might be the case of a large difference in density between the grains, *i.e.*, very light large grains and heavy small grains. The patterns obtained with the model are shown in the two lower panels in Figure 8. The late stage in the dynamics evolution of the patterns shown at the left lower panel ($\theta_{ll} - \theta_{ss} < 0$) and at the right lower panel ($\theta_{ll} - \theta_{ss} > 0$) in Figure 8 resemble the patterns of normal grading climbing ripples (Fig. 7a) and cross-stratification (Fig. 7b) respectively. This indicates the dominance of avalanche segregation (shape segregation and percolation effect) over the hopping induced segregation in this region of the phase space (this dominance is the opposite of what we find in the region $l_s - l_l > l_s$). However, as seen in Figure 8, these patterns appear only in the late stages of the evolution. As seen in the two lower panels, in the early stages the lamination structure appears to be dominated by the hopping induced segregation. We observe a clear transition at intermediate time in the simulation which can be clearly observed in the change of the climbing angle of the ripples observed in the left and right lower panels in Figure 8. The late stage patterns appear only when the slip-face is well developed after a transient of small ripples dominated by hopping segregation. We are not aware of any wind tunnel experiment or field observation showing similar dynamical transition, so it would be interesting to explore this transition experimentally.

4 Summary

In summary, we have shown that lamination in sedimentary rocks at around the centimeter scale is a manifestation of grain size and grain shape segregation. Thin layers of coarse and fine sand are present in these rocks, and understanding how layers in sandstone are created might aid, for instance, in oil exploration since great amounts of oil are locked beneath layered rocks. Our findings suggest a unifying framework towards the understanding of the origin of inverse grading, normal grading and cross-stratification patterns in wind ripple deposits. We identify the conditions under which these different laminations patterns arise in sandstone. In particular, we find that cross-stratification is only possible when the large grains are coarser than the small grains composing the layered structure in agreement with recent experiments on avalanche segregation in two-dimensional sandpiles. The fact that cross-stratification patterns are very common

in Nature might be due to the fact that fragmentation processes usually leads to smaller grains more rounded than larger grains. So far we have explored a two-dimensional cross-section of the ripple deposits. Extensions to three dimensional systems are ongoing as new physics may emerge when taking into account the lateral motion of the grains [21].

References

1. R.A. Bagnold, *The Physics of Blown Sand and Desert Dunes* (Chapman and Hall, London, 1941).
2. R.P. Sharp, J. Geol. **71**, 617 (1963).
3. R.E. Hunter, Sedimentol. **34**, 361 (1977).
4. H. Blatt, G. Middleton, R. Murray, *Origin of Sedimentary Rocks* (Prentice-Hall, New Jersey, 1980).
5. H.-E. Reineck, I.B. Singh, *Depositional Sedimentary Environment* (Springer-Verlag, Berlin, 1980).
6. D.M. Rubin, R.E. Hunter, Sedimentol. **29**, 121 (1982).
7. J.R.L. Allen, *Sedimentary Structures: Their Character and Physics Basis* (Elsevier, Amsterdam, 1984).
8. G.A. Kocurek, in *Sedimentary Environments: Processes, Facies, and Stratigraphy*, edited by H.G. Reading (Blackwell Science, Oxford, 1996), p. 125.
9. C.J. Schenk, in *Aeolian Sediments and Processes*, edited by M.E. Brookfield, T.S. Ahlbrandt (Elsevier, Amsterdam, 1983), p. 41.
10. B.T. Werner, D.T. Gillespie, Phys. Rev. Lett. **71**, 3230 (1993).
11. M. Seppälä, K. Lindé, Geogr. Ann. A **60**, 29 (1978).
12. R.S. Anderson, Earth Sci. Rev. **29**, 77 (1990).
13. R.S. Anderson, K.L. Bunas, Nature **365**, 740 (1993).
14. R.L. Brown, J. Inst. Fuel **13**, 15 (1939).
15. J.C. Williams, Univ. Sheffield Fuel Soc. J. **14**, 29 (1963).
16. H.A. Makse, S. Havlin, P.R. King, H.E. Stanley, Nature **386**, 379 (1997).
17. J.E. Ungar, P.K. Haff, Sedimentol. **34**, 289 (1987).
18. R.S. Anderson, P.K. Haff, Science **241**, 820 (1988).
19. S.B. Forrest, P.K. Haff, Science **255**, 1240 (1992).
20. R.S. Anderson, Sedimentol. **34**, 943 (1987).
21. W. Landry, B.T. Werner, Physica D **77**, 238 (1994).
22. O. Terzidis, P. Claudin, J.-P. Bouchaud, Eur. Phys. J. B **5**, 245 (1998).
23. J.-P. Bouchaud, M.E. Cates, J.R. Prakash, S.F. Edwards, Phys. Rev. Lett. **74**, 1982 (1995); J. Phys. I France **4**, 1383 (1994).
24. H.A. Makse, P. Cizeau, H.E. Stanley, Phys. Rev. Lett. **78**, 3298 (1997); P. Cizeau, H.A. Makse, H.E. Stanley, Phys. Rev. E **59**, 4408 (1999).
25. T. Boutreux, P.-G. de Gennes, J. Phys. I France **6**, 1295 (1996).
26. P.-G. de Gennes, C.R. Acad. Sci. (Paris) **321**, 501 (1995); P.-G. de Gennes, in *The Physics of Complex Systems* [Proc. Int'l School of Physics "Enrico Fermi" Course CXXXIV], edited by F. Mallamace, H.E. Stanley (IOS Press, Amsterdam, 1997).
27. Notice that all the quantities of the model are averaged over a coarse-grained scale of the order of a few grain sizes.
28. N. Vandewalle, S. Galam, Int. J. Mod. Phys. C **10** (to appear).
29. R. Cuerno, H.A. Makse, S. Tomassone, S.T. Harrington, H.E. Stanley, Phys. Rev. Lett. **75**, 4464 (1995).
30. S.B. Savage, C.K.K. Lun, J. Fluid Mech. **189**, 311 (1988).
31. T. Boutreux, H.A. Makse, P.-G. de Gennes, Eur. Phys. J. B **9**, 105 (1999).
32. H.A. Makse, Phys. Rev. E **56**, 7008 (1997).